Sample Corrugation Affects the Apparent Bond Lengths in Atomic Force Microscopy

Mark P. Boneschanscher,[†,§] Sampsa K. Hämäläinen,[‡,§] Peter Liljeroth,[‡,*] and Ingmar Swart[†,*]

[†]Debye Institute for Nanomaterials Science, Utrecht University, P.O. Box 80000, 3508TA Utrecht, The Netherlands and [‡]Department of Applied Physics, Aalto University School of Science, P.O. Box 15100, 00076 Aalto, Finland. [§]These authors contributed equally.

ABSTRACT Frequency modulation atomic force microscopy (AFM) allows the chemical structure of planar molecules to be determined with atomic resolution. Typically, these measurements are carried out in constant-height mode using carbon monoxide (CO) terminated tips. Such tips exhibit considerable flexibility, *i.e.*, the CO molecule can bend laterally due to the tip–sample interaction. Using epitaxial graphene as a model system, we demonstrate experimentally that the apparent atomic positions measured by AFM depend on the sample corrugation. Using molecular mechanics simulations, we explain these observations by the interplay of the CO bending and the nonlinear background signal arising from the neighboring atoms. These effects depend nontrivially on the tip–sample distance and limit the achievable accuracy on the bond length determination based on AFM experiments.

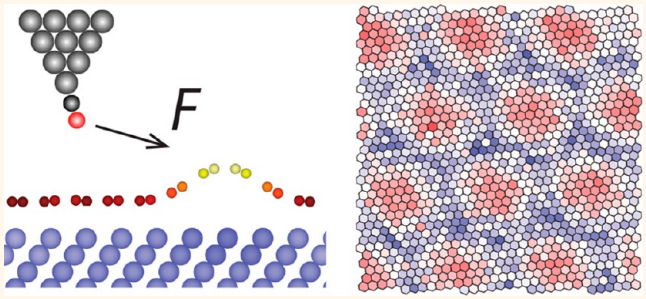

KEYWORDS: atomic force microscopy · bond length · tip relaxation · corrugation · graphene

Imaging individual planar molecules with atomic resolution is possible using frequency modulation atomic force microscopy (FM-AFM).[1−10] Besides structure determination, AFM can also provide more quantitative information. For example, different atomic species can be identified,[11−13] and the charge distribution inside a single molecule can be measured.[3] Recently, it was shown that the apparent height and length of bonds in planar molecules is correlated to the bond order.[4] It is even possible to visualize intermolecular hydrogen bonding using AFM.[14] Because of these new capabilities, AFM imaging with CO terminated tips finds increasing use in chemistry, molecular electronics, and materials science.[2,7,8,10,15,16]

In all cases where atomic resolution imaging of molecules was demonstrated, the experiments were performed in constant height mode. In this mode, the tip is raster scanned over the surface on a fixed plane, *i.e.*, the tip does not follow the corrugation of the surface. Instead, the frequency shift is measured as a function of position. In addition, in all experiments, chemically passivated tips were used, typically a carbon monoxide (CO) molecule adsorbed on the apex. Inert tips are essential to avoid accidental pick-up of the molecule of interest by the tip at the small distances and oscillation amplitudes required for atomic resolution imaging. The geometry of the CO in the junction depends on the tip–sample distance and on the crystallographic termination of the tip apex.[16,17] Attractive van der Waals and repulsive Pauli interactions can cause the CO molecule to bend.[16,18,19] The direction of this bending depends also on the neighboring atoms: if their positions are not symmetric with respect to the atom directly under the AFM tip, there is a nonsymmetric background force on the CO. This lateral force causes the CO molecule to bend and results in an apparent change of the bond length. The quantitative details of how nonplanarity and the associated degree of CO bending and background forces from the neighboring atoms affect the bond lengths extracted from AFM using CO terminated tips have not been established. Knowledge of these details is

* Address correspondence to l.swart@uu.nl, peter.liljeroth@aalto.fi.

Received for review January 17, 2014 and accepted February 23, 2014.

Published online February 23, 2014
10.1021/nn500317r

essential in assessing the experimentally achievable certainty in the bond lengths extracted from AFM measurements. This has a direct consequence for the use of AFM as a tool in single molecule structural chemistry and molecular electronics.

Here, we study experimentally and computationally how accurately the atomic positions can be extracted from AFM measurements using CO terminated tips. We use epitaxial graphene[20,21] as a model system. This material is ideally suited for this investigation as, due to a lattice mismatch between graphene and the Ir(111) substrate, the epitaxial layer exhibits a periodic physical buckling. The vertical corrugation is small enough to allow simultaneous atomic resolution imaging of both the top and valley sites in constant height mode.[21,22] In addition, the exact atomic scale structure of this system is known.[20,23−25]

RESULTS AND DISCUSSION

The structure of graphene on Ir(111) as adapted from dynamic low-energy electron diffraction (LEED-IV) measurements[20,25] is shown in Figure 1a. The lattice mismatch between the graphene layer and the underlying Ir(111) substrate gives rise to a moiré pattern. Different regions of the moiré unit cell have different graphene to Ir(111) registries, and we follow the common practice in naming these areas: top (graphene hexagon on top of an underlying Ir atom), fcc and hcp regions within the moiré pattern.[20,26] A schematic of the AFM experiment is shown in Figure 1b, and an example of a constant-height AFM image obtained with a CO tip is shown in Figure 1c. Besides the clear honeycomb arrangement of the carbon atoms, the

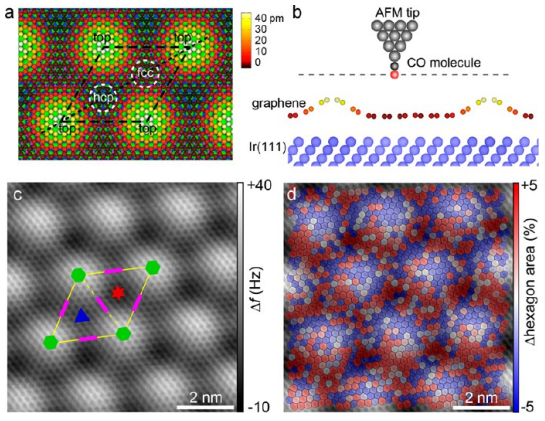

Figure 1. AFM experiments on epitaxial graphene on Ir(111): (a) structure of the graphene on Ir(111) surface, where the moiré unit cell and the regions with different average graphene−Ir(111) registries are indicated; (b) schematic of the AFM experiments with a CO-modified tip apex; (c) constant height AFM image of the graphene/Ir(111) substrate obtained on the repulsive branch of the Δf *vs* tip−sample distance curve using a CO-terminated tip. The moiré unit cell is indicated by yellow lines. Green hexagons indicate top sites, purple lines bridge sites and blue triangle and red star fcc and hcp sites, respectively. (d) Color coded map of the apparent graphene hexagon area.

periodic buckling of the graphene layer can be seen. This buckling corresponds to the moiré pattern.[20,25] The moiré unit cell is indicated in Figure 1c along with the different areas indicated in Figure 1a: 'top' (green hexagon), 'hcp'/'fcc' (red star/blue triangle) and bridge sites (purple line), respectively.

We analyzed the AFM data by extracting the area of each six-membered carbon ring (Methods). Figure 1d show the same image as Figure 1c, overlaid with hexagons color-coded to indicate the relative size of each cell compared to the average value. It is immediately clear that the hexagons at the moiré top sites are significantly smaller than the hexagons in the hcp and fcc sites. These deviations from average can be as large as ±15%. This implies that the C−C bonds at the top sites of the moiré pattern should be shorter than those at the hcp and fcc sites. A difference in area of ±15% approximately corresponds to an average difference in bond length of 20 pm.

The 3D structure of graphene on Ir(111) has been established by both LEED-IV and DFT calculations.[20,23−25] Both methods indicate that the variation in the C−C bond length across the moiré unit cell is very small: the difference between the shortest and longest bond is less than 0.3 pm. This is in strong contrast to the AFM result, where the difference between the longest and shortest bond can be as large as 15% of the bond length. This difference is of the same order as the difference in the bond length of C−C single (154 pm) and aromatic double bonds (139 pm).[27] Such large differences between bonds in epitaxial graphene are unphysical. Considering the arguments outlined above, it is clear that the variations that we see in AFM are not due to actual differences in bond length but are instead related to the imaging mechanism. We would like to note here that the frequency shift on top of a bond in constant height mode has been used as an indicator for bond-order in addition to the bond length.[4] This parameter cannot be used for analyzing bonds on corrugated samples as it relies on constant tip-bond distance.

In constant height AFM experiments, there are several variables that affect apparent bond lengths. First, it is well-known that the CO at the tip apex is flexible and can bend in response to attractive van der Waals (vdW) and repulsive Pauli interactions.[4,18] As the tip−sample distance varies in the constant height mode (the sample is vertically corrugated), the CO bending will vary and this might give rise to the observed changes in the bond lengths. Second, when the tip is exactly on top of a carbon atom, the distance to the neighboring atoms will be different if the sample is corrugated. This will give rise to a different background contribution to the measured force, which will also shift the apparent atomic positions.

We have investigated these effects in detail by constructing a model of the AFM experiments based

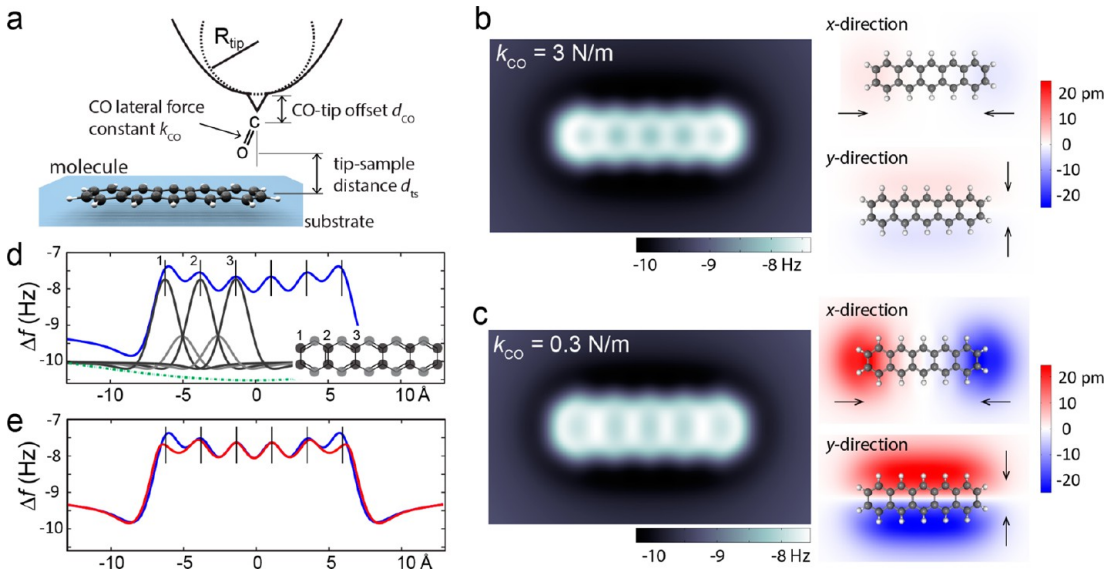

Figure 2. "Ball-and-stick" modeling of AFM imaging with a CO-terminated tip: (a) schematic of the model setup and the relevant parameters; (b and c) simulated constant height AFM images of pentacene (left) with a relatively stiff (b, k_{CO} = 3 N/m) and soft (c, k_{CO} = 0.3 N/m) CO lateral force constant and the corresponding maps of the CO bending (right). The arrows indicate the direction of the CO bending. (d) Extracted line profile along the center of the pentacene molecule for a nonflexible tip. The contributions from the individual dimers (black and gray lines, the corresponding atoms are indicated in the inset) and the overall van der Waals background between the CO molecule and the pentacene (green dotted line) have been shifted for clarity. (e) Extracted line profiles along the center of the pentacene molecule for the tips considered in panels b and c (blue and red lines correspond to lateral force constants of 3 and 0.3 N/m, respectively).

on molecular mechanics force field between a CO molecule and the sample (see Methods for details). The model system is depicted in Figure 2a. The main tunable parameters are the lateral spring constant of the CO molecule at the tip apex (k_{CO}), the bulk tip radius of curvature (R_{tip}), and the offset between the CO molecule and the bulk tip apex (d_{CO}, due to, for example, the presence of a metal cluster at the end of the tip). The latter two parameters mostly affect the depth of the minimum of the Δf *vs* tip−sample distance (d_{ts}) curves. These have been selected such that reasonable agreement with experimental results is obtained. While this model is more simplistic than the DFT calculations performed in, for example, refs 4, 18, 28, 29, the major advantage of the force field based modeling is that we can freely vary the lateral spring constant of the CO molecule at the tip apex, and thereby study the influence of the tip flexibility. In DFT calculations, this number is fixed by the choice of the metal cluster used as a tip model. Previous studies suggest the spring constant to be of the order of 0.1−3 N/m[4,16,17] and we explore this range to assess its effect on the measured response. Finally, to facilitate direct comparison with experimental results, we convert the calculated force cube into Δf data.[30,31]

To validate the simulations and to check the predictions on a well-studied model system, we have first considered a pentacene molecule adsorbed directly on a metal (Figure 2). We do not take into account electrostatic forces in the present case as these are not expected to qualitatively change the contrast formation mechanisms in the case of neutral molecules or graphene. These effects should naturally be included when considering molecules with charge centers or a net dipole moment. Calculated constant height Δf maps with two different lateral spring constants are shown in Figure 2b,c. Both strongly resemble experimental AFM images of pentacene. Especially the result obtained with the smaller k_{CO} is in essentially quantitative agreement with the experiment.[1] The simulations accurately reproduce the three main experimental observations of deviations between the real pentacene bond lengths and the apparent bond lengths in the AFM experiments: (1) all the phenyl rings are elongated in the *y*-direction;[1] (2) the left and rightmost phenyl rings are also elongated in the *x*-direction;[1] (3) as the tip−sample distance is reduced, the bonds appear sharper in the constant height Δf maps.[4]

The right panels of Figure 2b,c show the tip bending in the *x*- and *y*-direction for the stiffer and softer tips, respectively. The overall bending at the outer edge of the molecule is always toward the center of the molecule and is caused by the attractive vdW interaction between the CO molecule and the pentacene. A more detailed investigation reveals changes when going over the atoms as well: the tip can bend away from the nearest atom irrespective of the vdW background at sufficiently short tip−sample distances. The maximum tip displacement is of the order of a couple of picometers for the stiffer tip, but can reach several tens of picometers for the softer tip. This naturally

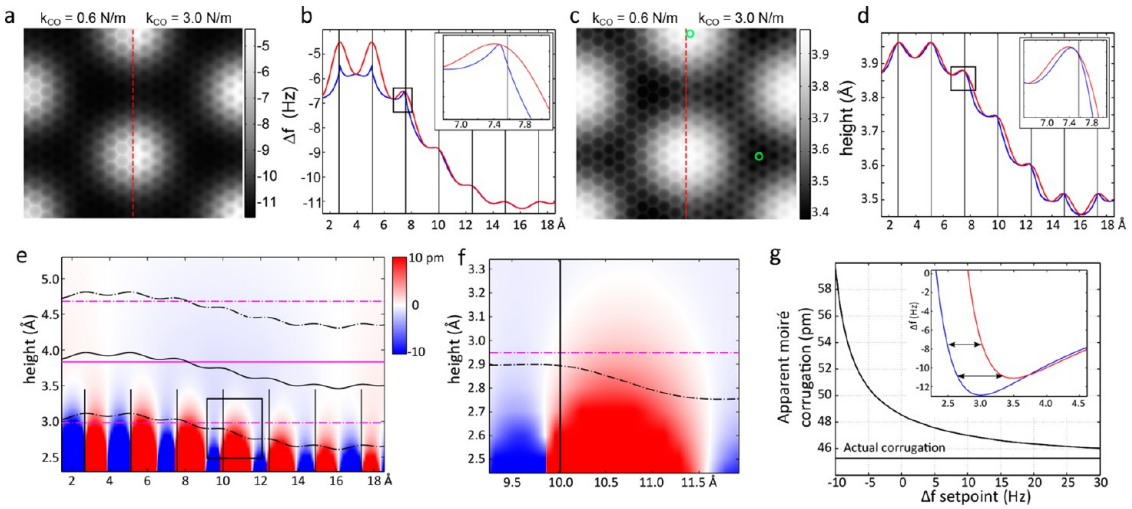

Figure 3. Simulated AFM images for the graphene moiré. (a) Simulated constant height images (average tip height with respect to the graphene top site is 3.8 Å) with a soft (left, k_{CO} = 0.6 N/m) and a stiff (right, k_{CO} = 3 N/m) tip. (b) Cross section from the constant height image in panel a taken along the dotted line from top to bridge site for the two CO spring constants (blue, 0.6 N/m; red, 3 N/m). The black lines mark the real positions of the bonds in the input file for the simulation. The inset shows a close up of one the bonds. (c) Simulated constant frequency shift images (at $\Delta f = -8$ Hz) with a soft (left, k_{CO} = 0.6 N/m) and a stiff (right, k_{CO} = 3 N/m) tip. (d) Cross section along dotted line in panel c from top to bridge site for the two CO spring constants (blue, 0.6 N/m; red, 3 N/m). The black vertical lines denote the actual positions of the bonds. The inset shows a close up of one the bonds. (e) Bending of the CO along the same section as shown in panels b and d (with k_{CO} = 3 N/m). The solid lines correspond to the tip height (black line at $\Delta f = -8$ Hz and magenta line at constant height of 3.8 Å), while the dotted lines show the limits of the oscillation (A = 0.85 Å). (f) Close-up of the bending near one of the bonds (indicated with a square in panel e). (g) Apparent corrugation of the graphene moiré as a function of the Δf set point on the repulsive side of the Δf *vs* d_{ts} for a nonflexible tip. The inset shows $\Delta f - d_{ts}$ curves simulated at the points marked with green circles in panel c.

depends on the tip−sample distance, with the CO bending more at smaller d_{ts}.

Before discussing the effect of CO bending in detail, we will first investigate how the background forces from the neighboring atoms affect the apparent atomic positions. Figure 2d shows an extracted Δf line profile (blue line) along the center of the pentacene molecule for a nonflexible tip ($k_{CO} = \infty$). The peaks in Δf correspond to the *apparent* positions of the carbon dimers along the middle of the pentacene molecule. Their *real* positions are marked by vertical lines. The contributions to the total Δf signal from the individual dimers are given by the black solid lines (the gray lines give the response of the outermost carbon atoms, see inset for a schematic). The green dotted line gives the overall van der Waals attraction between the bulk Ir tip and the pentacene molecule.

It is immediately obvious that the peaks corresponding to the left and rightmost carbon atoms are shifted toward the center of the molecule. This effect is large (the lateral shift is around 25 pm), and it is due to the asymmetric background signal from the neighboring atoms. The AFM measures the total Δf, and the signal from the neighboring atoms (the last dimer has neighboring atoms on only one side) causes an apparent shift in the position of the C−C bond. The peak corresponding to dimer 2 is also shifted toward the left, *i.e.*, the outermost benzene ring is contracted on both sides. This small shift (around 5 pm depending on the tip height) is due to the slope of the vdW background between the tip and whole pentacene molecule. This effect is of course also present on the last dimer, but there the asymmetry in the neighboring atoms has the dominant contribution. In planar molecules, these effects will always cause an apparent contraction toward the center of the molecule of the outermost rings.

Finally, Figure 2e compares the extracted Δf line profiles along the center of the pentacene molecule for stiff (k_{CO} = 3 N/m, blue line) and soft (k_{CO} = 0.3 N/m, red line) CO tips. The results obtained with the stiffer tip are quantitatively very close to the nonflexible tip discussed in Figure 2d. As k_{CO} becomes smaller, the bending of the CO increases. In general, the vdW attraction causes the molecule to bend toward the center of the pentacene. As a result, the outermost bonds appear stretched, both in *x*- and *y*-directions. Hence, the effect of tip flexibility is opposite to that of the asymmetric background forces. Which effect is dominant depends on the lateral force constant of the CO and on the tip−sample distance. Note that it is problematic to assess the effect of tip flexibility by DFT calculations, due to the difficulties in varying k_{CO}.

Having established the different mechanisms affecting the apparent locations of the bonds, we now turn to the buckled graphene moiré. Figure 3a shows a simulated constant height image of graphene/Ir(111) surface using coordinates adapted from LEED-I(V) experiments.[25] The left-hand side of the image is obtained with a lateral spring constant of 0.6 N/m

and the right-hand side with 3 N/m. With the softer tip one can clearly see the sharpening of the bonds caused by the CO bending away from the carbon atoms near the top sites of the moiré where the tip−sample distance is the smallest. Comparison of the simulated and experimental images suggests that the tip in these experiments on graphene on Ir was laterally stiffer than the tip used for the experiments on pentacene.[1] A variation in the lateral spring constant is not surprising, as the stiffness depends on the exact atomic configuration of the tip and also on the on the tip material.[4] Here, the tip apex is likely to be coated by iridium atoms compared to the Cu tip used in the pentacene experiment.

We find that the CO at the tip apex generally bends toward the top sites due to the increased vdW attraction, in line with what we observed for the pentacene molecule. However, near the top sites of the moiré the tip−sample distance is smaller, causing the tip to flip from side to side when going over the carbon bonds. This results in bonds that appear sharper on the top sites in the constant height image. This sharpening is clearly seen in Figure 3a and in the cross section shown in Figure 3b. The effect of the CO bending on the apparent bond lengths is difficult to observe directly in the simulated constant height images. This is caused by the fact that the same background will shift broader peaks more than sharp ones. While the local maximum of the Δf signal for the softer tip (blue line) is closer to the real atomic position (shift 11 pm in Figure 3b inset) than with the stiffer tip (shift 17 pm in Figure 3b inset), it is impossible to deconvolve the effects of the bond sharpening effect and the tip bending toward the top site, as both will always be present.

As can be seen in Figure 3b, the bonds shift toward the nearest top site for both tip stiffnesses. Hence, benzene rings near the moiré top sites appear smaller, which is in qualitative agreement with the experimental data shown in Figure 1d. The effect is similar to pentacene imaged with a stiff tip, where the nonhomogeneous contribution from the neighboring atoms to the Δf signal dominates over the tip bending. The neighboring atoms around the moiré top site are closer to the tip and thus have a larger contribution to Δf signal. Hence, the contribution from the neighboring atoms to the total Δf signal can be positive, even when the force between the tip and these atoms is attractive.

The AFM can also be operated in feedback mode where the frequency shift Δf is kept constant by adjusting the height of the tip relative to the sample. To first order, this eliminates the spatial variation of the tip−sample distance for corrugated samples. Hence, the degree of the CO bending as the tip passes over a substrate atom should no longer be spatially dependent. As such, constant frequency shift experiments and simulations can give further insight into which factors are dominant for determining atomic positions. Figure 3c shows two simulated constant Δf images with different CO spring constants (0.6 and 3 N/m) at $\Delta f = -8$ Hz (in the repulsive branch of the Δf *vs* d_{ts}). Compared to the constant height images in Figure 3a, the atomic corrugation is more uniform across the unit cell since in constant-frequency shift mode the tip effectively follows the surface contours. As can be seen in Figure 3d, the bonds are slightly contracted toward the top sites similarly to the constant height case. The softer tip is again closer to the true positions with the different bonds being shifted by 4−16 pm compared to 6−28 pm for the stiffer tip. Going closer to the sample by increasing the Δf set point decreases the shift somewhat, but even when going extremely close, the bonds on the sloping part of the moiré are still shifted by over 10 pm. At very close distances, the CO bending actually reverses: the CO starts bending outward from the moiré top sites (Figure 3e,f). This is the point where the CO finally starts to feel repulsion from the neighboring atoms. With a set point of −8 Hz, the tip just barely reaches this area where it bends outward on top of the underlying bond at the very bottom of its oscillation cycle (dotted line in Figure 3e). Whether this point is reached at a given Δf depends largely on the shape of the bulk tip and the oscillation amplitude of the tip.

Contrary to the constant height mode where the bonds appeared sharpest near the moiré top sites, the bonds in constant Δf are sharpest near the moiré hcp and fcc sites. This is especially clear for the softer tip (left-hand side in Figure 3c). The sharpness of the bonds is a consequence of a smaller tip-graphene distance. The reason for the tip being pushed closer is the increase of the long-range vdW forces from the bulk tip. Even if the repulsive part of the force increases very sharply at close distances, the additive character of the vdW forces combined with the sheer size of the bulk tip is enough to push it closer. This effect is similar the one reported previously, where the modeling was done in the attractive side of the Δf−d_{ts} slope and, hence, caused an inverse effect (underestimation of the moiré corrugation).[32]

To study how accurately AFM can measure height differences in cases where the background forces change, we plotted the apparent height difference between the topmost and lowest atoms of the moiré (marked with green circles in Figure 3c) as a function of the Δf set point. The resulting curve with a nonflexible tip is shown in Figure 3g. At Δf set points corresponding to the bottom of the Δf−d_{ts} curve, the moiré corrugation is overestimated significantly. As the tip−sample distance is reduced, the apparent corrugation gradually decreases toward the geometric corrugation. However, in the span of set points we have studied, it never reaches the true corrugation of *ca.* 45 pm, but remains firmly some picometers above this

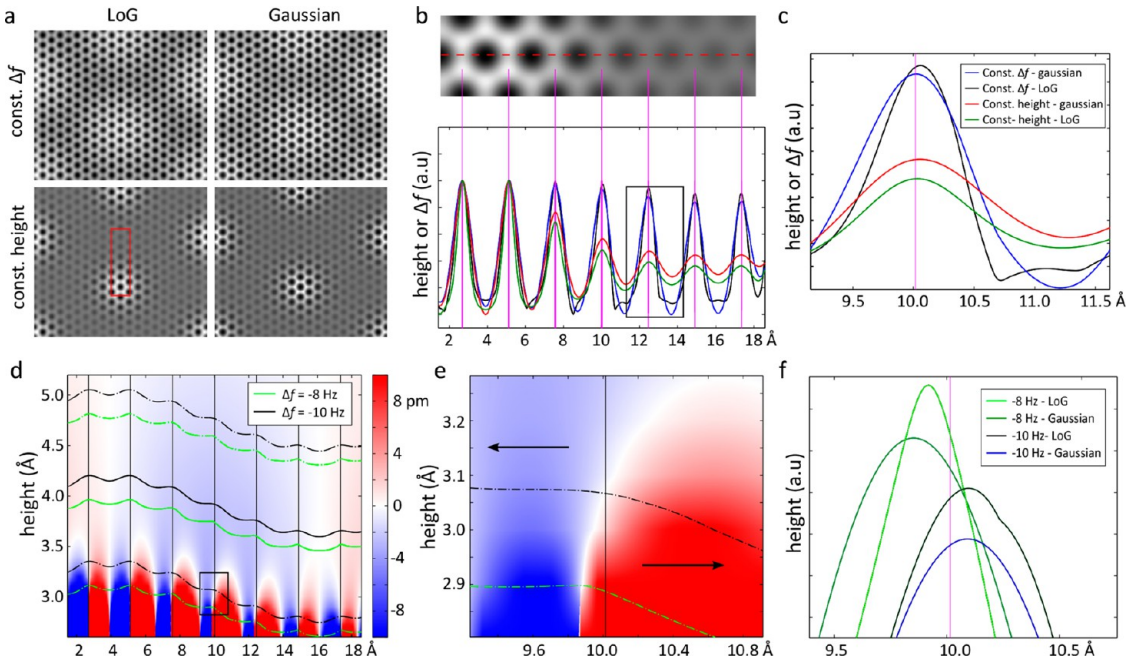

Figure 4. The effect of background subtraction on the apparent bond positions in simulated AFM images with a stiff tip (k_{CO} = 3 N/m). (a) Background subtracted constant Δf (Δf = 0 Hz) and constant height (average tip height 3.65 Å) images using either a heavily Gaussian blurred background (σ = 1 Å) or a Laplacian of Gaussians filter (σ = 0.6 Å). (b) Normalized cross sections of the images in panel a in the red square. The vertical lines mark the positions of the bonds. (c) Zoom-in on one of the bonds showing how the bonds on the constant height image are shifted out from the top sites. (d) Cross section along the same line for a more flexible tip (k_{CO} = 0.6 N/m) calculated at two different Δf set points. The background color corresponds to the bending of the CO along the same section. (e) Close-up of the bending in the area marked with a square in panel d. (f) Zoom-in to the background corrected cross section on the same bond after background subtraction for the two different Δf set points.

level. With reasonable values of Δf, the corrugation is overestimated by almost 10%. The magnitude of the overestimation depends again on the bulk tip shape and the tip oscillation amplitude.

Awareness of the background forces arising from the substrate is also necessary in measuring adsorption geometries of molecules on surfaces. For example, when the molecule adsorbs in a nonplanar configuration, the background force has to be considered for a correct determination of the angle between the molecular plane and the substrate.[28] In the case of molecules, this background force can be simply measured on the bare substrate adjacent to the molecule,[28] which is difficult for extended two-dimensional layers such as graphene.

According to our simulations, both constant height and constant frequency shift AFM measurements detect apparent changes in the atomic positions on corrugated surfaces. As explained above, in the case of the graphene on Ir(111) experiments, we get best correspondence between theory and experiment when using a relatively large lateral spring constant. The apparent changes in the atomic positions are then caused by the asymmetric background signal from the neighboring atoms that are at different heights. This suggests that an appropriate background correction or subtraction could remedy the situation and allow us to extract the actual atomic positions from the experiments. We have tested this idea using the simulations and the results are summarized in Figure 4. We have removed the moiré corrugation from the simulated images using different filtering schemes. Examples on the results of background subtracted constant frequency shift and constant height images are shown in Figure 4a. Here, the background was removed by either estimating the background by blurring out the atomic corrugation with a Gaussian and subtracting this from the original image or with a Laplacian of Gaussians (LoG) filter which removes the long wavelength moiré corrugation (it essentially gives the second derivative of the sample corrugation). Note that both methods are generally applicable for any a priori unknown background with a periodicity that is larger than the atomic corrugation.

Figure 4b shows cross-sectional profiles of the background corrected images for two different filtering schemes. A zoom-in on one of the bonds is shown in Figure 4c. As can be seen in the images, background subtraction of AFM images results in an apparent expansion of the top sites, *i.e.*, the trend from noncorrected data is reversed. In both the constant frequency shift and constant height data, background correction improves the match between the apparent and real bond positions. The apparent positions in background corrected data can be as close as 1 pm from the real bond positions; however, typically, the difference is of the order of 3−5 pm. While these differences depend on the exact form of the background,

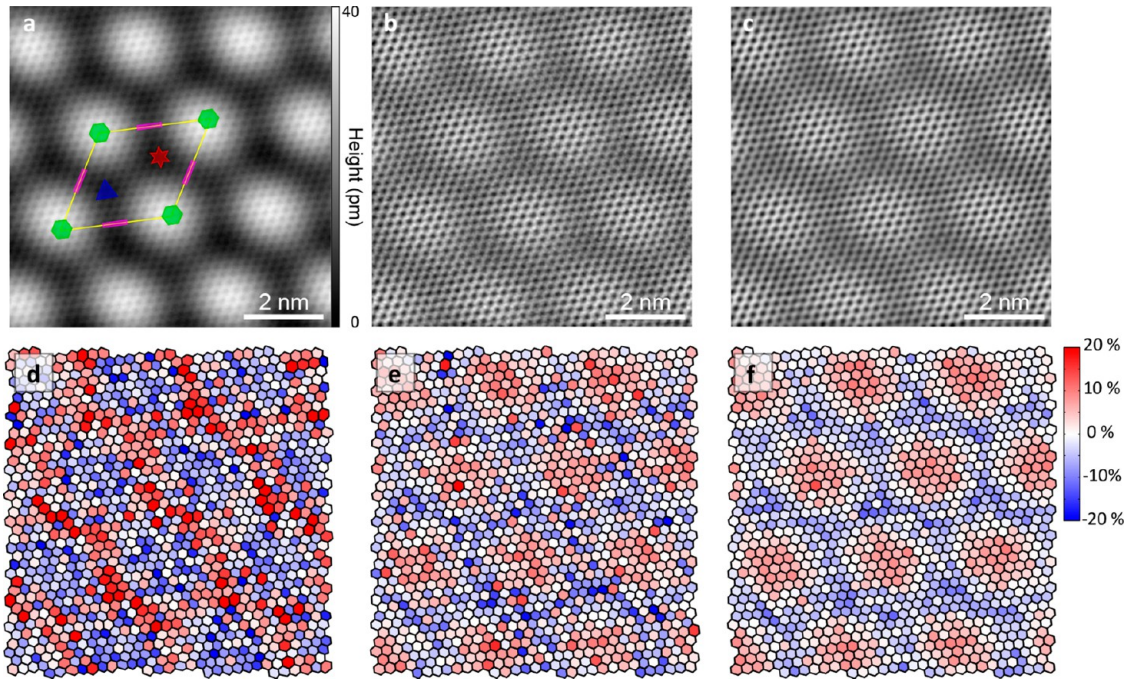

Figure 5. Effect of background subtraction on the experimental AFM images: (a) constant frequency shift AFM image of graphene on Ir(111) with a CO terminated tip obtained at a feedback set point of $\Delta f = 0$; (b and c) image from panel a after background subtraction using Gaussian blurring with $\sigma = 1$ Å (b) or a Laplacian of a Gaussian with $\sigma = 0.6$ Å (c); (d and f) color coded maps of the apparent graphene hexagon area as extracted from the constant frequency shift image in panel a (d), or background subtracted images in panels b (e) and c (f).

the tip−sample distance, and the lateral force constant of the tip, it appears that using the Gaussian blurred image as the background in constant frequency shift images results in very accurate estimation of the bond positions to within <2 pm.

As the background subtraction significantly reduces the effect of the background forces, we are now able to study the effect of the CO bending on the graphene moiré. To enhance the effect of CO bending, we have calculated two constant frequency shift images with a softer tip (k_{CO} = 0.6 N/m). Figure 4d shows a height cross section along the same line as in the previous panels calculated with two different Δf set points (−8 and −10 Hz on the repulsive branch). The main difference is that, at $\Delta f = -8$ Hz, the CO reaches the region where it starts to bend away from the top sites (red background) at the bottom of its oscillation cycle, while in the $\Delta f = -10$ Hz image, the CO remains bent toward the top site over the full oscillation cycle. This can clearly be seen in the zoomed-in image in Figure 4e. Figure 4f shows the cross section of the same zoom-in after background correction with the two methods described above. In the case of the $\Delta f = -8$ Hz image, the bonds now appear closer to the top site, whereas for the $\Delta f = -10$ Hz image, they are farther from it. This is in line with the tip bending away and toward the top site, respectively. In addition, the flexibility of the CO causes the bonds to appear sharper at the shorter tip−sample distance. Since this also has a slight effect on the apparent bond positions after background subtraction, the bond shift in Figure 4f cannot fully be attributed to the tip bending alone. However, the shift in Figure 4f is *ca.* 20 pm, which is larger than the typical shifts due to changes in the peak shape.

We can demonstrate the effect of the background subtraction in the experimental images as shown in Figure 5. A constant frequency shift AFM image of the graphene on Ir(111) surface acquired with a CO-terminated tip is shown in Figure 5a. Background subtracted images using the Gaussian blurred background and LoG filtering are shown in Figure 5, panels b and c, respectively. The extracted apparent hexagon areas are displayed in Figure 5d−f. It is apparent that the trend of smaller top sites is reduced, and even reversed in the background corrected data, consistent with the LoG filtered simulated images. The remaining differences in the apparent hexagon areas (±5%) convert into ±3 pm changes in the graphene bond lengths. This is close to the results from the simulated images and close to the typical noise levels of a low-temperature scanning probe microscope.

CONCLUSIONS

We have studied the influence of sample corrugation on the determination of the bond-lengths by noncontact AFM with a CO-terminated tip. For corrugated samples, the precision is limited by the background forces arising from the neighboring atoms and the flexibility of the CO at the tip apex. Using epitaxial graphene as a model

system, we demonstrate experimentally and by the use of molecular mechanics simulations that the asymmetric background forces are the limiting factor in our experiments. While nonbackground corrected data gives errors of the order 20 pm in the atomic positions, suitable background correction can reduce this to the level of a couple of picometers for a relatively stiff tip. Our work has a direct bearing on the accuracy of total structure determination at the single molecule level using noncontact AFM with functionalized tips.

METHODS

Graphene Growth. Epitaxial graphene on Ir(111) was grown from ethylene using the temperature programmed growth method.[33−37] The Ir(111) surface was cleaned by repetitive cycles of argon sputtering and flash heating to 1500 K. After the sample had cooled below 570 K, ethylene was deposited on the surface (3×10^{-6} mbar for 10 s). The temperature was then increased to 1200 K for 20 s to grow large, mostly defect free graphene islands.

AFM Experiments. The experiments were done using a low-temperature STM/AFM (T = 4.8 K, Omicron Nanotechnology GmbH) and a quartz based tuning fork sensor in the qPlus design. The microscope is housed within the same ultrahigh vacuum system (base pressure $<10^{-10}$ mbar) as the sample preparation system. Commercially available qPlus force sensors with mounted W tips were used (resonance frequency f_0 of *ca.* 24.5 kHz, a quality factor of 12 000, and a peak to peak oscillation amplitude of *ca.* 170 pm). All images were taken with a bias voltage of 0 V.

Tip Preparation. The metal tip apex was formed by controlled contact with the iridium surface, resulting in an iridium coated metal tip. The metallic nature of the tip was confirmed by conductance spectroscopy on the iridium surface. CO terminated tips were prepared by leaking CO into the vacuum chamber ($P_{max} \sim 10^{-9}$ mbar) and opening the doors in the radiation shields for 10 s. This often resulted in a CO terminated tip, as evidenced by the absence of the contrast inversion in constant height imaging at various heights.[21]

Bond Length Determination. To determine the bond lengths, we used a combination of template matching, Voronoi analysis, and spline fitting using MATLAB. First, the experimental images are averaged over forward and backward scan direction and filtered with a Gaussian filter ($\sigma \leq 1$ Å) to remove 'salt-and-pepper' noise. A spherical mask is created, consisting of a dark ring matching the size of the hollow sites of the hexagons and a bright ring around it. The correlation coefficient for each pixel of the image is calculated according to

$$\rho_{AB} = \frac{\langle AB \rangle - \langle A \rangle \langle B \rangle}{\sigma_A \sigma_B}$$

where $\sigma_A = \langle A^2 \rangle - \langle A \rangle^2$, $\sigma_B = \langle B^2 \rangle - \langle B \rangle^2$, and A and B are the intensities of mask and masked area of the image, respectively. The resulting correlation image was binarized at a value of typically +0.35 and segmented by means of connected-component labeling. Finally, the centers of the hexagons were detected by taking the center of mass of each image segment. Then, a Voronoi analysis was used to detect the nearest neighbors of each hexagon. The lines connecting each hexagon to its nearest neighbors were extracted as height/intensity profiles. The maximum of these profiles was detected by spline fitting, giving us the center position of each carbon−carbon bond in the image. The positions of the carbon atoms were then detected as the intersection of lines fitted through these points.

AFM Image Simulations. A MATLAB code was used to simulate the CO bending and calculate the forces on the tip after CO relaxation. All forces were modeled with a Lennard-Jones-type 9−6 potential.[38] Four different force components were taken into account, namely, CO−graphene, CO−bulk Ir substrate, bulk tip−graphene, and bulk tip−bulk Ir substrate. To relax the CO, the forces exerted on it were calculated in vector format while for the other forces only the z-component was taken into account. The bulk tip was modeled as a continuum Ir sphere with a radius of 10 nm. Analytic formulas derived based on ref 39 were used to calculate the bulk forces at each point. In simulations on graphene, the CO molecule was offset by 6 Å from the spherical bulk tip in order to mimic a micro tip most likely present in the measurements. This offset was set to zero in the simulations involving pentacene.

The forces were calculated in a cube with a typical step size of around 5 pm in all directions. For the cross sections, a lateral step size of 1 pm was used. Only the force on the oxygen atom of the CO was taken in to account in the relaxation. The oxygen atom was allowed to move on the spherical surface with a radius defined by the sum of the CO adsorption height and the bond length (3 Å). The displacement of the oxygen used in calculating the spring force of the CO was taken along the spherical surface, *i.e.*, not directly as the lateral displacement. The CO was relaxed self-consistently in each point of the cube until the lateral displacement between iterations was less than 5 fm or when the maximum of 80 iterations was reached. Usually, the forces converged well before the maximum number of iterations was reached. Only at extremely close tip−sample distances was the maximum number of iterations reached in some cases.

Conflict of Interest: The authors declare no competing financial interest.

Acknowledgment. Fruitful discussions with J. van der Lit and D. Vanmaekelbergh are acknowledged. This research was supported by The Netherlands Organization for Scientific Research (Chemical Sciences, Veni-grant 722.011.007), the Foundation for Fundamental Research on Matter ["Control over Functional Nanoparticle Solids"], the European Research Council (ERC-2011-StG No. 278698 "PRECISE-NANO"), the Academy of Finland (Centre of Excellence in Low Temperature Quantum Phenomena and Devices No. 250280), and the Finnish Academy of Science and Letters.

REFERENCES AND NOTES

1. Gross, L.; Mohn, F.; Moll, N.; Liljeroth, P.; Meyer, G. The Chemical Structure of a Molecule Resolved by Atomic Force Microscopy. *Science* **2009**, *325*, 1110–1114.
2. Gross, L.; Mohn, F.; Moll, N.; Meyer, G.; Ebel, R.; Abdel-Mageed, W. M.; Jaspars, M. Organic Structure Determination Using Atomic-Resolution Scanning Probe Microscopy. *Nat. Chem.* **2010**, *2*, 821–825.
3. Mohn, F.; Gross, L.; Moll, N.; Meyer, G. Imaging the Charge Distribution within a Single Molecule. *Nat. Nanotechnol.* **2012**, *7*, 227–231.
4. Gross, L.; Mohn, F.; Moll, N.; Schuler, B.; Criado, A.; Guitián, E.; Peña, D.; Gourdon, A.; Meyer, G. Bond-Order Discrimination by Atomic Force Microscopy. *Science* **2012**, *337*, 1326–1329.
5. de Oteyza, D. G.; Gorman, P.; Chen, Y.-C.; Wickenburg, S.; Riss, A.; Mowbray, D. J.; Etkin, G.; Pedramrazi, Z.; Tsai, H.-Z.; Rubio, A.; *et al.* Direct Imaging of Covalent Bond Structure in Single-Molecule Chemical Reactions. *Science* **2013**, *340*, 1434–1437.
6. Guillermet, O.; Gauthier, S.; Joachim, C.; de Mendoza, P.; Lauterbach, T.; Echavarren, A. Stm and Afm High Resolution Intramolecular Imaging of a Single Decastarphene Molecule. *Chem. Phys. Lett.* **2011**, *511*, 482–485.
7. Pavliček, N.; Fleury, B.; Neu, M.; Niedenführ, J.; Herranz-Lancho, C.; Ruben, M.; Repp, J. Atomic Force Microscopy Reveals Bistable Configurations of Dibenzo[a,H]Thianthrene and Their Interconversion Pathway. *Phys. Rev. Lett.* **2012**, *108*, 086101.

8. Albrecht, F.; Neu, M.; Quest, C.; Swart, I.; Repp, J. Formation and Characterization of a Molecule−Metal−Molecule Bridge in Real Space. *J. Am. Chem. Soc.* **2013**, *135*, 9200–9203.
9. van der Lit, J.; Boneschanscher, M. P.; Vanmaekelbergh, D.; Ijäs, M.; Uppstu, A.; Ervasti, M.; Harju, A.; Liljeroth, P.; Swart, I. Suppression of Electron−Vibron Coupling in Graphene Nanoribbons Contacted *via* a Single Atom. *Nat. Commun.* **2013**, *4*, 2023.
10. Riss, A.; Wickenburg, S.; Gorman, P.; Tan, L. Z.; Tsai, H.-Z.; de Oteyza, D. G.; Chen, Y.-C.; Bradley, A. J.; Ugeda, M. M.; Etkin, G.; *et al.* Local Electronic and Chemical Structure of Oligo-Acetylene Derivatives Formed through Radical Cyclizations at a Surface. *Nano Lett.* **2014**, 10.1021/nl403791q.
11. Sugimoto, Y.; Pou, P.; Abe, M.; Jelinek, P.; Perez, R.; Morita, S.; Custance, O. Chemical Identification of Individual Surface Atoms by Atomic Force Microscopy. *Nature* **2007**, *446*, 64–67.
12. Welker, J.; Weymouth, A. J.; Giessibl, F. J. The Influence of Chemical Bonding Configuration on Atomic Identification by Force Spectroscopy. *ACS Nano* **2013**, *7*, 7377–7382.
13. Lantz, M. A.; Hug, H. J.; Hoffmann, R.; van Schendel, P. J. A.; Kappenberger, P.; Martin, S.; Baratoff, A.; Güntherodt, H.-J. Quantitative Measurement of Short-Range Chemical Bonding Forces. *Science* **2001**, *291*, 2580–2583.
14. Zhang, J.; Chen, P.; Yuan, B.; Ji, W.; Cheng, Z.; Qiu, X. Real-Space Identification of Intermolecular Bonding with Atomic Force Microscopy. *Science* **2013**, *342*, 611–614.
15. Mohn, F.; Repp, J.; Gross, L.; Meyer, G.; Dyer, M.; Persson, M. Reversible Bond Formation in a Gold-Atom-Organic-Molecule Complex as a Molecular Switch. *Phys. Rev. Lett.* **2010**, *105*, 266102.
16. Weymouth, A. J.; Hofmann, T.; Giessibl, F. J. Quantifying Molecular Stiffness and Interaction with Lateral Force Microscopy. *Science* **2014**, 10.1126/science.1249502.
17. Welker, J.; Giessibl, F. J. Revealing the Angular Symmetry of Chemical Bonds by Atomic Force Microscopy. *Science* **2012**, *336*, 444–449.
18. Sun, Z.; Boneschanscher, M. P.; Swart, I.; Vanmaekelbergh, D.; Liljeroth, P. Quantitative Atomic Force Microscopy with Carbon Monoxide Terminated Tips. *Phys. Rev. Lett.* **2011**, *106*, 046104.
19. Mohn, F.; Schuler, B.; Gross, L.; Meyer, G. Different Tips for High-Resolution Atomic Force Microscopy and Scanning Tunneling Microscopy of Single Molecules. *Appl. Phys. Lett.* **2013**, *102*, 073109.
20. Busse, C.; Lazić, P.; Djemour, R.; Coraux, J.; Gerber, T.; Atodiresei, N.; Caciuc, V.; Brako, R.; N'Diaye, A. T.; Blügel, S.; *et al.* Graphene on Ir(111): Physisorption with Chemical Modulation. *Phys. Rev. Lett.* **2011**, *107*, 036101.
21. Boneschanscher, M. P.; van der Lit, J.; Sun, Z.; Swart, I.; Liljeroth, P.; Vanmaekelbergh, D. Quantitative Atomic Resolution Force Imaging on Epitaxial Graphene with Reactive and Non-Reactive Afm Probes. *ACS Nano* **2012**, *6*, 10216–10221.
22. Dedkov, Y.; Voloshina, E. Multichannel Scanning Probe Microscopy and Spectroscopy of Graphene Moire Structures. *Phys. Chem. Chem. Phys.* **2014**, *16*, 3894–908.
23. Meng, L.; Wu, R.; Zhang, L.; Li, L.; Du, S.; Wang, Y.; Gao, H.-J. Multi-Oriented Moiré Superstructures of Graphene on Ir(111): Experimental Observations and Theoretical Models. *J. Phys.: Condens. Matter* **2012**, *24*, 314214.
24. Voloshina, E. N.; Fertitta, E.; Garhofer, A.; Mittendorfer, F.; Fonin, M.; Thissen, A.; Dedkov, Y. S. Electronic Structure and Imaging Contrast of Graphene Moire on Metals. *Sci. Rep.* **2013**, *3*, 1072.
25. Hämäläinen, S. K.; Boneschanscher, M. P.; Jacobse, P. H.; Swart, I.; Pussi, K.; Moritz, W.; Lahtinen, J.; Liljeroth, P.; Sainio, J. Structure and Local Variations of the Graphene Moiré on Ir(111). *Phys. Rev. B* **2013**, *88*, 201406.
26. N'Diaye, A. T.; Coraux, J.; Plasa, T. N.; Busse, C.; Michely, T. Structure of Epitaxial Graphene on Ir(111). *New J. Phys.* **2008**, *10*, 043033.
27. Lide, D. R. *Handbook of Chemistry & Physics*, 83rd ed.; CRC Press LLC: Boca Raton, FL, 2002.
28. Schuler, B.; Liu, W.; Tkatchenko, A.; Moll, N.; Meyer, G.; Mistry, A.; Fox, D.; Gross, L. Adsorption Geometry Determination of Single Molecules by Atomic Force Microscopy. *Phys. Rev. Lett.* **2013**, *111*, 106103.
29. Moll, N.; Gross, L.; Mohn, F.; Curioni, A.; Meyer, G. The Mechanisms Underlying the Enhanced Resolution of Atomic Force Microscopy with Functionalized Tips. *New J. Phys.* **2010**, *12*, 125020.
30. Giessibl, F. J. Forces and Frequency Shifts in Atomic-Resolution Dynamic-Force Microscopy. *Phys. Rev. B* **1997**, *56*, 16010–16015.
31. Sader, J. E.; Jarvis, S. P. Accurate Formulas for Interaction Force and Energy in Frequency Modulation Force Spectroscopy. *Appl. Phys. Lett.* **2004**, *84*, 1801–1803.
32. Sun, Z.; Hämäläinen, S. K.; Sainio, J.; Lahtinen, J.; Vanmaekelbergh, D.; Liljeroth, P. Topographic and Electronic Contrast of the Graphene Moire on Ir(111) Probed by Scanning Tunneling Microscopy and Noncontact Atomic Force Microscopy. *Phys. Rev. B* **2011**, *83*, 081415.
33. Coraux, J.; N'Diaye, A. T.; Engler, M.; Busse, C.; Wall, D.; Buckanie, N.; Meyer zu Heringdorf, F.-J.; van Gastel, R.; Poelsema, B.; Michely, T. Growth of Graphene on Ir(111). *New J. Phys.* **2009**, *11*, 023006.
34. Subramaniam, D.; Libisch, F.; Li, Y.; Pauly, C.; Geringer, V.; Reiter, R.; Mashoff, T.; Liebmann, M.; Burgdörfer, J.; Busse, C.; *et al.* Wave-Function Mapping of Graphene Quantum Dots with Soft Confinement. *Phys. Rev. Lett.* **2012**, *108*, 046801.
35. Pletikosic, I.; Kralj, M.; Pervan, P.; Brako, R.; Coraux, J.; N'Diaye, A. T.; Busse, C.; Michely, T. Dirac Cones and Minigaps for Graphene on Ir(111). *Phys. Rev. Lett.* **2009**, *102*, 056808.
36. Lacovig, P.; Pozzo, M.; Alfé, D.; Vilmercati, P.; Baraldi, A.; Lizzit, S. Growth of Dome-Shaped Carbon Nanoislands on Ir(111): The Intermediate between Carbidic Clusters and Quasi-Free-Standing Graphene. *Phys. Rev. Lett.* **2009**, *103*, 166101.
37. Altenburg, S. J.; Kröger, J.; Wehling, T. O.; Sachs, B.; Lichtenstein, A. I.; Berndt, R. Local Gating of an Ir(111) Surface Resonance by Graphene Islands. *Phys. Rev. Lett.* **2012**, *108*, 206805.
38. Yang, J.; Ren, Y.; Tian, A.-M.; Sun, H. Compass Force Field for 14 Inorganic Molecules, He, Ne, Ar, Kr, Xe, H_2, O_2, N_2, NO, CO, CO_2, NO_2, CS_2, and SO_2, in Liquid Phases. *J. Phys. Chem. B* **2000**, *104*, 4951–4957.
39. Hamaker, H. C. The London—van der Waals Attraction between Spherical Particles. *Physica* **1937**, *4*, 1058–1072.